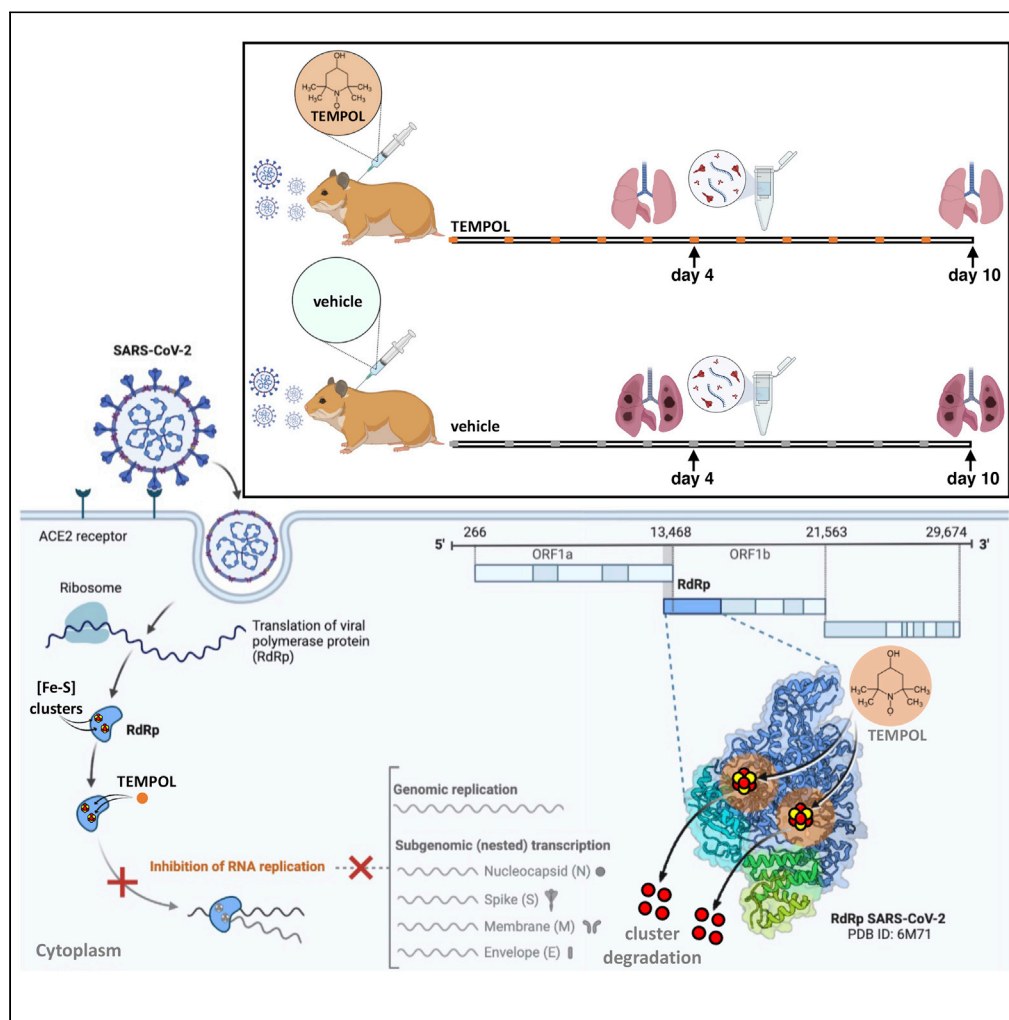


Article

TEMPOL inhibits SARS-CoV-2 replication and development of lung disease in the Syrian hamster model



Nunziata Maio, Sara Cherry, David C. Schultz, Brett L. Hurst, W. Marston Linehan, Tracey A. Rouault

rouault@mail.nih.gov

Highlights

TEMPOL's IC_{50} in human lung epithelial Calu-3 cells is $2.89 \mu\text{M}$ and $CC_{50} > 10 \text{ mM}$

TEMPOL has potent antiviral activity against highly pathogenic SARS- and MERS-CoVs

TEMPOL inhibits SARS-CoV-2 replication and lung pathology in the Syrian hamster

Fe-S cofactor insertion can be targeted to interfere with coronavirus replication

Article

TEMPOL inhibits SARS-CoV-2 replication and development of lung disease in the Syrian hamster model

Nunziata Maio,¹ Sara Cherry,² David C. Schultz,³ Brett L. Hurst,⁴ W. Marston Linehan,⁵ and Tracey A. Rouault^{1,6,*}

SUMMARY

Severe acute respiratory syndrome coronavirus 2 (SARS-CoV-2) has caused a worldwide outbreak, known as coronavirus disease 2019 (COVID-19). Alongside vaccines, antiviral therapeutics is an important part of the healthcare response to COVID-19. We previously reported that TEMPOL, a small molecule stable nitroxide, inactivated the RNA-dependent RNA polymerase (RdRp) of SARS-CoV-2 by causing the oxidative degradation of its iron-sulfur cofactors. Here, we demonstrate that TEMPOL is effective *in vivo* in inhibiting viral replication in the Syrian hamster model. The inhibitory effect of TEMPOL on SARS-CoV-2 replication was observed in animals when the drug was administered 2 h before infection in a high-risk exposure model. These data support the potential application of TEMPOL as a highly efficacious antiviral against SARS-CoV-2 infection in humans.

INTRODUCTION

Human coronavirus infections are common, with at least four examples (229E, NL63, OC43 and HKU1) now considered endemic (Corman et al., 2018). However, the emergence during the past twenty years of SARS-CoV-1, MERS-CoV (Middle East Respiratory Syndrome coronavirus), and SARS-CoV-2 highlights the significant threat potential of this viral class. Severe acute respiratory syndrome coronavirus 2 (SARS-CoV-2) is the causal agent of coronavirus disease 2019 (COVID-19) (Lu et al., 2020), which was declared a pandemic by the World Health Organization (WHO) on March 11, 2020 and has resulted in 503 million confirmed cases with over 6 million deaths globally as of March 2022. SARS-CoV-2 is a highly infectious, RNA beta coronavirus that can cause adult respiratory distress syndrome in the most serious cases. Although effective vaccines have been developed with unprecedented timelines, a significant number of people are either unable or unwilling to be vaccinated and global access challenges remain. Limited therapeutic options are available to those who are infected. Repurposing of approved drugs in the search for small molecule antiviral agents that target SARS-CoV-2 has thus far been minimally effective (Consortium et al., 2021; Riva et al., 2020). Vaccination with the SARS-CoV-2 spike protein, regardless of the technology platform, induces an immune response that significantly reduces hospitalization and deaths, even to variants of concern (VOC) that have thus far emerged (including Omicron) (Thompson et al., 2022). Similarly, monoclonal antibodies and small molecule drugs for COVID-19 were developed rapidly and have proven effective in preventing serious diseases (Edwards et al., 2022). The aim of antiviral therapies is to halt the progression of COVID-19 before patients advance to more serious acute and/or chronic diseases. To this end, both antibody (delivered by injection or intravenously) and drug approaches (delivered as a pill or intravenously) have been pursued. The three antiviral drugs in use, which inhibit SARS-CoV-2 replication, were initially developed in antiviral programs that focused on treatment for other viruses. They include molnupiravir (Gordon et al., 2021) and remdesivir (Gordon et al., 2020), which act on the RNA-dependent RNA polymerase, and an analog of a previously developed protease inhibitor, PF07321332, in combination with the CYP3A4 inhibitor ritonavir, marketed as Paxlovid, which inactivates the main protease (Owen et al., 2021) required to cleave functional proteins from the long polypeptide that the virus initially synthesizes. The development of COVID-19 therapeutics has been guided by our increasing understanding of the timing of SARS-CoV-2 infection and COVID-19. Once infected and depending on the variant and the immune status of the individual, SARS-CoV-2 replication occurs in the upper respiratory tract for 1 to 4 days before the onset of symptoms and peaks before or during the early phases of symptomatic disease. The virus is difficult to isolate following day 7 after symptomatic disease (Munster et al., 2020; Sauter et al.,

¹Molecular Medicine Branch, Eunice Kennedy Shriver National Institute of Child Health and Human Development, National Institutes of Health, Bethesda, MD 20892, USA

²Department of Pathology and Laboratory Medicine, Chemogenomic Discovery Program, University of Pennsylvania, Perelman School of Medicine, Philadelphia, PA 19104, USA

³Department of Biochemistry and Biophysics, High-throughput Screening Core, University of Pennsylvania, Perelman School of Medicine, Philadelphia, PA 19104, USA

⁴Institute for Antiviral Research, Utah State University, Logan, UT 84322, USA

⁵Urologic Oncology Branch, Center for Cancer Research, National Cancer Institute, Bethesda, MD 20892, USA

⁶Lead contact

*Correspondence: rouault@mail.nih.gov

<https://doi.org/10.1016/j.isci.2022.105074>



2020; Woolsey et al., 2021), but the viral genome can be detected for 2 to 3 additional weeks. Early-stage acute infection often is mild and resolves in most people; however, in some cases, a more serious infection of the lower respiratory tract occurs, which induces an immunopathogenic phase that emerges around 7 to 10 days after symptomatic disease. Extensive dysregulation of the immune system during this immunopathologic stage can lead to lung damage, blood clotting, and acute respiratory distress syndrome (ARDS), which is a severe end-stage lung disease with ~30% mortality rates (Kumar et al., 2020).

Oral anti-SARS-CoV-2 therapeutics are needed to prevent more severe disease, hospitalization, and death. Early treatment is also expected to reduce the period of infectivity. We recently identified TEMPOL (4-hydroxy-2,2,6,6-tetramethylpiperidine-N-oxyl), a small molecule stable nitroxide, as a potent inhibitor of SARS-CoV-2 replication *in vitro* based on its ability to oxidize and degrade two newly identified iron-sulfur (Fe-S) cofactors in the catalytic subunit, nsp12, of the RNA-dependent RNA polymerase (RdRp) (Maio et al., 2021). Fe-S clusters are inorganic cofactors composed of iron and inorganic sulfur that are known to be highly susceptible to oxidative degradation (Imlay, 2006; Rouault and Maio, 2020). Previous studies have shown that TEMPOL was safe and beneficial in two different animal models of human conditions through its ability to oxidize and disassemble the Fe-S cluster of cytosolic aconitase (aka IRP1), which was converted into the Iron Responsive Element-binding apo-form (Ghosh et al., 2008, 2018). Given the pivotal role of SARS-CoV-2 RdRp in viral replication, it is unlikely that mutations will develop that interfere with Fe-S cluster ligation. Therefore, targeting the RdRp with TEMPOL represents an attractive approach for antiviral therapy to treat COVID-19.

In this study, we determined the half-maximal inhibitory concentration (IC₅₀) value for TEMPOL in tissue culture and subsequently assessed its antiviral potency in controlling SARS-CoV-2 infection following subcutaneous injection in the highly susceptible Syrian hamster model (Chan et al., 2020; Rosenke et al., 2020). We show that TEMPOL when administered 2 h prior to SARS-CoV-2 infection significantly decreased viral lung loads and pathology, without affecting shedding from the upper respiratory tract. These findings support the potential of TEMPOL as a drug for patients who have experienced a high-risk exposure or developed early COVID-19.

RESULTS

TEMPOL inhibits SARS-CoV-2 replication in human lung epithelial Calu-3 cells

We determined the *in vitro* inhibitory effect of TEMPOL on SARS-CoV-2 replication in Calu-3 cells, a pre-clinically relevant human lung epithelial cell line. Calu-3 cells were pretreated with TEMPOL for 2 h before continuous infection with SARS-CoV-2 (isolate USA WA1/2020) at a MOI of 0.5. Forty-eight hours post-infection, cells were fixed, immunostained, and imaged by automated microscopy for infection and cell number. The half-maximal inhibitory concentration (IC₅₀) value for TEMPOL was 1.45 μ M and 90% inhibitory concentration (IC₉₀) was 2.89 μ M (Figure 1A). Viability was assessed over the differing concentrations, demonstrating the absence of cellular toxicity at the highest drug concentration tested of 20 μ M (Figure 1B), though higher concentrations of up to 10 mM were well tolerated by Calu-3 cells (Figure 1C).

As TEMPOL's antiviral activity against SARS-CoV-2 was exerted through its ability to oxidize and disassemble the iron-sulfur cofactors in the RdRp (Maio et al., 2021) and because the iron-sulfur ligating residues in the SARS-CoV-2 RdRp are conserved among zoonotic and human coronaviruses (Maio et al., 2021), we evaluated the *in vitro* cellular antiviral activity of TEMPOL against SARS-CoV and MERS coronavirus using cytopathic effect (CPE) assays (Tables S1 and S2). We found that TEMPOL demonstrated potent antiviral activity against SARS-CoV with an EC₅₀ of 46 μ M, and MERS-CoV with an EC₅₀ of 73 μ M, in their respective cellular assays (Tables S1 and S2).

Syrian hamster model-study design

Having verified *in vitro* the antiviral activity of TEMPOL, we assessed its efficacy in the Syrian hamster model, which is regarded as a preclinical model of mild disease, with animals developing mild to moderate interstitial pneumonia following infection in a high-risk exposure system (Chan et al., 2020; Rosenke et al., 2020). Hamsters were infected intranasally with SARS-CoV-2 (USA-WA1/2020) using a dose of 1×10^5 TCID₅₀ (100,000 times the infectious dose 50; ID₅₀). The ID₅₀ value was determined in a separate study centered on the refinement of the Syrian hamster model for SARS-CoV-2 infection studies (Rosenke et al., 2020).

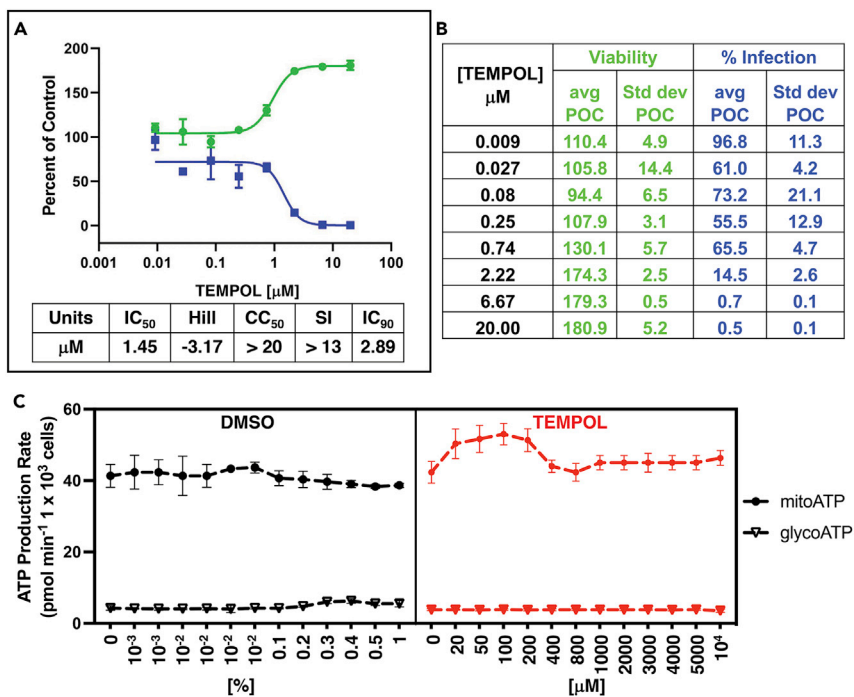


Figure 1. TEMPOL inhibits SARS-CoV-2 replication in human lung epithelial Calu-3 cells

(A) Calu3 (ATCC, #HTB-55) cells were pretreated with TEMPOL for 2 h prior to continuous infection with SARS-CoV-2 (isolate USA WA1/2020) at MOI = 0.5. Forty-eight hours post-infection, cells were fixed, immunostained, and imaged by automated microscopy for infection (dsRNA + cells/total cell number) and cell number. TEMPOL-treated well data were normalized to aggregated DMSO control wells and plotted versus drug concentration to determine the IC₅₀ (infection: blue) and CC₅₀ (toxicity: green) (data are expressed as mean ± SD; n = 3 biological replicates). (Inset) Half-maximal inhibitory concentration (IC₅₀), 50% cytotoxic concentration (CC₅₀), selectivity index (SI) and 90% inhibitory concentration (IC₉₀) of TEMPOL (units are 10⁻⁶ M).

(B) Viability and percentage of infection in Calu-3 cells treated with the indicated concentrations of TEMPOL (0.01-20 μM) for 2 h before continuous infection with SARS-CoV-2 (isolate USA WA1/2020) at an of MOI = 0.5. Values represent average Percentage of Control (POC) = (TEMPOL well measurements/aggregated DMSO average) * 100 (n = 3 biological replicates).

(C) Calu-3 cell viability on treatment with up to 10 mM TEMPOL was assessed with the real-time ATP rate assay kit (Agilent). ATP production rates from glycolysis (glycoATP) and oxidative phosphorylation (mitoATP) were simultaneously determined with a Seahorse XFe96 Analyzer. As a control, the viability of cells treated with DMSO alone used to dissolve TEMPOL, were also included (data are expressed as mean ± SD; n = 3 biological replicates).

One group of hamsters (n = 8, comprising 4 males and 4 females) received TEMPOL subcutaneously at 50 mg/kg b.i.d. for the first three days post-infection, followed by a single dose of 25 mg/kg from day 4 through day 9 (Figure 2). A control group (n = 8, comprising 4 males and 4 females) was treated using the same route and timing as the TEMPOL group with vehicle only (see schematic; Figure 2). Treatment in all groups was continued for nine consecutive days. Four hamsters per group were euthanized on day 4 post-infection at the peak of virus replication (Rosenke et al., 2020) and 4 per group on day 10.

This dosing regimen was based on previous studies in mice, in which intravenous injection of 5 μL/g of body weight of a 150 mM solution of TEMPOL in PBS (PBS), with an injection volume of 115-150 μL depending on the weight of the mouse (corresponding to a 3.2 mg dose for an average mouse of 25 g) led to a maximum blood concentration of 8.1 ± 1.3 mM TEMPOL (Davis et al., 2011), which exceeds the calculated IC₉₀ of 2.89 μM by three orders of magnitude. The maximum concentration achieved was the lowest in the muscle (0.6 ± 0.1 mM) and highest in the kidney (7.2 ± 0.5 mM). A maximum concentration of 2.0 ± 0.5 mM TEMPOL was detected in the salivary glands (Davis et al., 2011), which is more than 600-fold higher than the IC₉₀, suggesting that therapeutically efficacious doses of TEMPOL can be achieved in the oral cavity, an important site for SARS-CoV-2 entry and a potential route of SARS-CoV-2 transmission (Huang et al., 2021). TEMPOL can be delivered effectively in oral form, as mice fed a diet containing 10 mg of

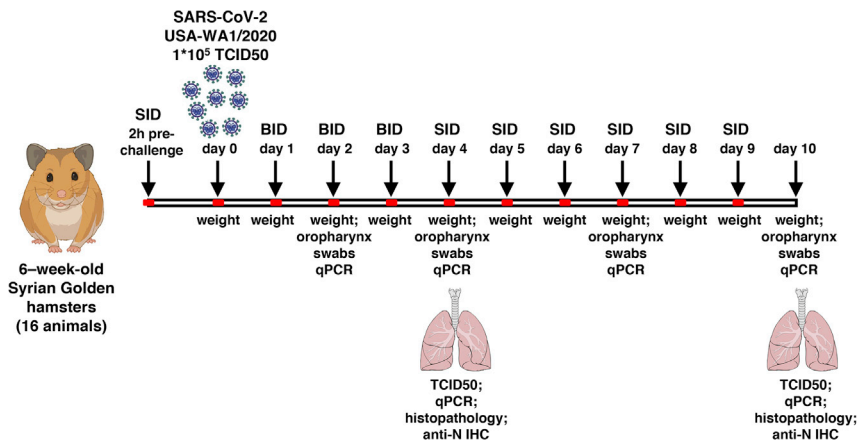


Figure 2. Syrian hamster model-study design

Hamsters were intranasally inoculated with SARS-CoV-2 (USA WA1/2020 at a dose of 10^5 TCID₅₀). Sixteen 6–8-week-old Golden Syrian hamsters in an equal number of males (8) and females (8), were acclimated for 11 days on arrival and divided into 2 groups of 8 ($n = 8$) per group. On day 0, all animals were challenged intranasally with SARS-CoV-2. Before the challenge (2hrs pre-challenge), animals were treated subcutaneously (SQ) with 50 mg/kg TEMPOL (SID). Animals were treated at 12 additional timepoints thereafter; BID for the first three days at 50 mg/kg TEMPOL and then once a day (SID) from day 4 through day 9 at 25 mg/kg in accordance with the study design shown. In-life blood collections were performed at 2 separate timepoints, pre-treatment and pre-challenge on day 0. Animals' weights and clinical observations were recorded every day. During the challenge period, hamsters were weighed once daily and clinically observed twice a day. Hamsters had oral swabs taken on days 2, 4, 7, and 10. Cardiac punctures and tissue collections occurred on day 4 ($n = 2$ /grp/sex; total $n = 4$ per group) and on day 10 ($n = 2$ /grp/sex; total $n = 4$ per group). Collected nasal turbinates and lungs were weighed and processed as follows: left lungs were preserved in 10% neutral buffered formalin (NBF) for histopathology; and right lungs and nasal turbinates (sectioned at least 0.1–0.2 g) were snap-frozen for viral load through qPCR assay and TCID₅₀.

TEMPOL per gram of food for two weeks had concentrations of $91.9 \pm 19.9 \mu\text{M}$ in the blood; $40.1 \pm 22.6 \mu\text{M}$ TEMPOL in the heart; $12.6 \pm 3.7 \mu\text{M}$ in the adipose tissue; $16.8 \pm 8.1 \mu\text{M}$ in the brain and $232.9 \pm 59.9 \mu\text{M}$ in the kidney (Ghosh et al., 2008), indicating that the oral administration of TEMPOL to mice leads to concentrations in the blood and in all the tested tissues that were well above the IC₉₀. The concentrations achieved were sufficient to activate the Iron Responsive Element (IRE) binding activity of IRP1 through the disassembly of its iron-sulfur cluster (Ghosh et al., 2008, 2018). No observable side effects were noted upon daily oral administration of TEMPOL to mice for more than 18 months (Ghosh et al., 2008, 2018).

In vivo efficacy of TEMPOL against SARS-CoV-2 infection in the upper respiratory tract

Disease in Syrian hamsters following SARS-CoV-2 infection usually peaks at or around 4 days post-infection (dpi) and clinical illness is manifested by weight loss and pathological changes in the lungs of the infected animals (Chan et al., 2020; Imai et al., 2020; Rosenke et al., 2020; Sia et al., 2020). As shown in Figure 3A, following infection with SARS-CoV-2, hamsters treated with TEMPOL were protected from weight loss versus vehicle-treated animals ($-6.05\% \pm 1.59$ TEMPOL-treated vs $-17.3\% \pm 2.0$ in vehicle-treated animals at day 6 post-infection). Virus shedding was measured in oropharyngeal swabs collected on days 2, 4, 7, and 10 post-infection. Levels of viral RNA in the oropharyngeal tract decreased from day 4 through 10 and were significantly lower in TEMPOL-treated animals on day 7 (Figures 3B and 3C; approximately 10^5 vs 10^3 in vehicle vs TEMPOL-treated animals). Although more variable, infectious titers recovered from turbinates were consistent with the genome copy data, as a trend toward decreased levels of infectious virus was detected in TEMPOL-treated hamsters on day 4 post-infection (Figure 3D).

Histopathological analysis of the lungs and virus titers in vehicle- and TEMPOL-treated animals

Histopathological analyses were performed on lung samples obtained by euthanizing a subset of animals 4 days post-infection, when viral replication and disease usually peak. One animal in the untreated group was euthanized on day 6 post-infection owing to extreme morbidity caused by the consolidation of more

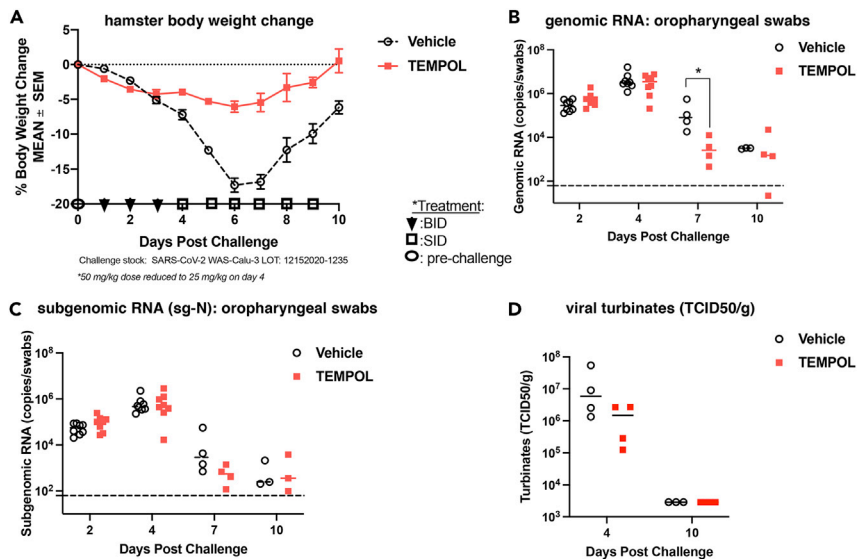


Figure 3. In vivo efficacy of TEMPOL against SARS-CoV-2 infection in the Syrian hamster model; body weight, virus shedding, viral loads, and infectious titers in the upper respiratory tract

Eight hamsters/group were challenged intranasally with 1×10^5 50% cell culture infectious doses of SARS-CoV-2. Animals were subcutaneously injected with 50 mg/kg TEMPOL or vehicle (placebo) twice daily (BID) for the first 3 days and once daily (SID) from day 4 through 9. Animals were euthanized on days 4 and 10 post-infection and lungs and turbinates were collected for virus titers.

(A) Animals were weighed daily. Weight loss is expressed as % of body weight change during the course of the infection. Data are expressed as mean \pm SD.

(B) Oropharyngeal swab samples ($n = 8$ /group on days 2 and 4; $n = 4$ /group on days 7 and 10) were collected on days 2, 4, 7, and 10 post-infection and viral shedding determined by RT-qPCR (p value vehicle vs TEMPOL-treated on day 7 = 0.0286, unpaired parametric two-tailed Welch's t test). The dashed line indicates the limit of detection. Data are expressed as mean \pm SD.

(C) Oropharyngeal swab samples ($n = 8$ /group on days 2 and 4; $n = 4$ /group on days 7 and 10) were collected on days 2, 4, 7, and 10 post-infection and subgenomic RNA levels of the N protein determined by RT-qPCR (no statistically significant difference was found between vehicle and TEMPOL-treated groups). The dashed line indicates the limit of detection. Data are expressed as mean \pm SD.

(D) Nasal turbinate samples were collected on days 4 and 10 post-infection ($n = 4$ per group), homogenized and titered for infectious virus (TCID₅₀) (Reed and Muench, 1938) on Vero E6 cells. Data are expressed as mean \pm SD. No statistically significant difference was found between vehicle- and TEMPOL-treated groups (unpaired parametric two-tailed Welch's t test, $p = 0.31$; $F = 309$).

than 80% of the lung (Figure S1). Microscopic findings in the lung of this animal included perivascular edema, alveolar hemorrhages, marked bronchioloalveolar hyperplasia, mixed cell alveolar inflammation, mild mononuclear cell vascular/perivascular inflammation, and scarce but observable formations of syncytia (Figure S1B). The pathologic changes were more extensive than those of other SARS-CoV-2 infected hamsters, and the animal was euthanized owing to severe morbidity.

The histopathologic findings differed markedly between TEMPOL-treated and -untreated infected animals (Figures 4A-4F and Table S3). Dark red lungs or dark patches were observed in both vehicle control and TEMPOL-treated animals on days 4 and/or day 10 post-infection (Figures 4A-4D), but they were more extensive in vehicle-treated control animals, where macroscopic observations correlated microscopically to alveolar hemorrhage and bronchioloalveolar hyperplasia. Atelectasis, which is the complete or partial collapse of a lung lobe (Figures 4A and 4C) was considered an artifact in this study owing to insufficient insufflation of the lung with formalin when tissues were collected. In TEMPOL-treated animals, microscopic correlates consisted mainly of atelectasis (Figures 4B and 4D). See Table S3 for the grading scale of SARS-CoV-2-related pathological changes in each animal of the two experimental groups.

Untreated animals on day 4 post-infection exhibited edema, alveolar hemorrhages, bronchioloalveolar hyperplasia, and mixed mononuclear cell vascular/perivascular inflammation (Figures 4A and 4C). In contrast,

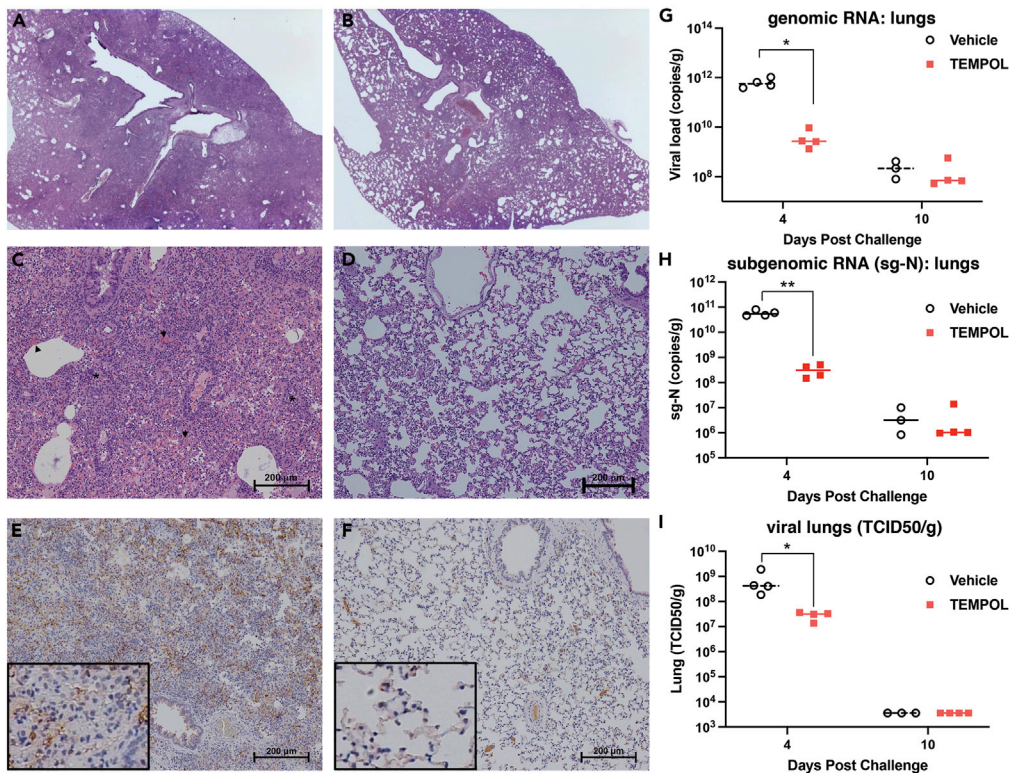


Figure 4. Histopathological analysis of the lung tissue and virus titers showed reduced pathology and viral loads in TEMPOL-treated animals (representative images are from female animals)

See Table S3 for the grading scale of SARS-CoV-2-related pathological changes in each animal of the two experimental groups. Hematoxylin and eosin (H&E) staining was used on lung sections to examine lung pathology post-inoculation. Immunohistochemistry (IHC) was used to detect the viral antigen nucleocapsid on lung sections from each animal (n = 4 per group).

(A, C, and E) Untreated vehicle controls at day 4 post-infection.

(B, D, and F) TEMPOL-treated animals. A, B. H&E stain (1.25 X) of vehicle (A) and TEMPOL-treated (B) animals.

(C and D) H&E stain (10 X) of vehicle (C) and TEMPOL-treated (D) animals. Panels A and C, (Group 1 corresponding to vehicle control animals), in the lungs, minimal to mild edema, minimal to mild alveolar hemorrhage (arrowhead), minimal to mild bronchioloalveolar hyperplasia (asterisk), mild to moderate mixed cell inflammation, and mild to moderate mononuclear cell vascular/perivascular inflammation were observed. Panels B and D, (Group 2 corresponding to TEMPOL-treated animals), in the lung, minimal bronchioloalveolar hyperplasia and mild mixed cell inflammation were observed. The incidence of SARS-CoV-2-related microscopic findings was mild to absent. Dark pink areas in images are caused by artifactual atelectasis owing to poor lung inflation at necropsy.

(E and F) Lung (10X). IHC for SARS-CoV-2 nucleocapsid antibody at day 4 post-infection. Numerous immunoreactive bronchiolar cells, type I and II pneumocytes, and fewer macrophages were detected in vehicle control animals (E). Immunoreactivity was strikingly reduced in TEMPOL-treated animals (F). Scale bar is 200 μ m.

(G) Lung virus loads (copies per gram of tissue) (n = 4 per group) were determined by RT-qPCR (p value vehicle control vs TEMPOL-treated at day 4 post-infection = 0.0214 by unpaired parametric two-tailed Welch's t test). Data are expressed as mean \pm SD.

(H) Lung subgenomic viral RNA encoding N protein was determined by RT-qPCR (n = 4 per group; p value vehicle control vs TEMPOL-treated at day 4 post-infection = 0.0052 by unpaired parametric two-tailed Welch's t test). Data are expressed as mean \pm SD.

(I) Infectious titers in the lungs (TCID₅₀) were significantly lower in TEMPOL-treated animals compared to vehicle controls. Data are expressed as mean \pm SD (p value vehicle control vs TEMPOL-treated at day 4 post-infection = 0.0286 by unpaired parametric two-tailed Welch's t test).

lungs of TEMPOL-treated hamsters manifested much less consolidation owing to hyperplasia and fluid accumulation and inflammation, as evidenced by the presence of numerous areas where the alveoli were preserved with intact air exchange surfaces (Figures 4B and 4D). At day 4 post-infection, there was a notable decreased incidence of vascular/perivascular mononuclear cell inflammation, hemorrhage,

and edema in TEMPOL-treated animals compared to vehicle controls; bronchioloalveolar hyperplasia was absent in females in the TEMPOL-treated group and significantly decreased in severity in males. The severity of incidence of mixed cell inflammation was significantly decreased in TEMPOL-treated animals.

At day 10 post-infection, SARS-CoV-2-related severity and/or incidence generally decreased overall in vehicle-treated animals, with the exception of bronchioloalveolar hyperplasia which increased in severity relative to day 4. In TEMPOL-treated animals, with the exception of one animal with minimal mixed cell inflammation, SARS-CoV-2-related microscopic findings were absent.

By day 10 post-infection, vehicle control animals were still abnormal (Figures S2A and S2B). SARS-CoV-2-related microscopic findings included bronchioloalveolar hyperplasia, mononuclear vascular/perivascular inflammation, alveolar hemorrhage, edema, mixed cell inflammation, syncytial cells, and pleural fibrosis. Conversely, TEMPOL-treated animals exhibited much less bronchioloalveolar hyperplasia and minimal mixed cell inflammation (Figures S2C and S2D).

Immunoreactivity against SARS-CoV-2 antigen was used to further compare the lung samples between the two different treatment groups (Figures 4E and 4F; S3A and S3B). Antigen staining with anti-nucleocapsid antibody was observed in the bronchial and bronchiolar epithelium, type I and II pneumocytes as well as a small number of pulmonary macrophages. A positive pixel analysis on whole lung slides demonstrated a significant difference in viral antigen present between the two groups. The total number of positive pixels was divided by the area of the slide scanned to determine the percentage of lung positive for the viral antigen. This analysis revealed that the vehicle controls contained on average 5.22 times more antigen than the TEMPOL-treated animals (Figure S4).

Viral titers were assessed in lung tissue samples collected at the peak of virus replication and disease, at day 4 post-infection. In contrast to levels of shedding in the upper respiratory tract (oropharyngeal), a 2-log decrease in viral RNA was detected in the lungs of TEMPOL-treated hamsters when compared to the vehicle control group (Figures 4G and 4H). This corresponded to a 1-log decrease in infectious virus in the lungs of TEMPOL-treated groups when compared to the vehicle controls (Figure 4I).

DISCUSSION

Here, we have shown that TEMPOL is an effective antiviral that mitigates lung disease in a well-characterized animal model of SARS-CoV-2 infection. We also established that low micromolar levels of TEMPOL are effective in blocking SARS-CoV-2 replication in a relevant human lung epithelial cell line. Owing to the mechanism of action of TEMPOL and the conservation of the iron-sulfur ligating centers among zoonotic and human pathogenic coronaviruses, we discovered that TEMPOL is also active against SARS-CoV and MERS-CoV infections in cell culture.

We used the established Syrian hamster model to assess whether TEMPOL treatment would mitigate COVID-19 *in vivo* in an animal model through its ability to inactivate the viral replicase. Our study shows that TEMPOL substantially reduced SARS-CoV-2 replication in the lungs based on both viral RNA genome copy number and levels of infectious virus. Importantly, the inhibition of viral replication by TEMPOL was associated with markedly reduced pathologic changes in the lungs. TEMPOL treatment reduced viral RNA by 2-logs and virus lung titers by 1-log, which was also confirmed by decreased SARS-CoV-2 nucleocapsid antigen levels in the lungs and by a substantial reduction of characteristic viral-induced pathological changes. Direct-acting antivirals are known to be most effective during the initial phase of illness characterized by rapid viral replication (Rosenke et al., 2021; Sheahan et al., 2017). Once viral replication ceases, some patients may develop a respiratory distress syndrome that results from an exuberant immune response elicited by the initial viral infection. Vaccination against SARS-CoV-2 is protective, although booster immunizations are needed to maintain immunity, which otherwise wanes within months. Moreover, current vaccines appear to be less protective from infection by recently emerging viral variants with more extensive variations in the S protein, such as Omicron, even after a third dose (Garcia-Beltran et al., 2022; Iketani et al., 2022; Sheward et al., 2022), owing to the focus of vaccine design toward spike protein sequences that prevailed in the initial phase of the pandemic. The three drugs that have thus far been approved by the FDA to inhibit SARS-CoV-2 replication are molnupiravir, remdesivir, and PF-07321332 (in Paxlovid). Remdesivir and molnupiravir are produced as pro-drugs; each is chemically modified to improve stability in blood and to promote efficient cellular uptake, and each is converted inside cells

into an active nucleoside competitor. PF-07321332 inhibits the main protease (Mpro). Its rapid inactivation by the CYP3A4 led to it being offered in combination with ritonavir, a CYP3A4 inhibitor safely used in several other protease-containing drug combinations, to extend half-lives of drugs metabolized by cytochrome P450 enzymes (Owen et al., 2021).

More antivirals that work through different mechanisms need to be developed to manage the SARS-CoV-2 and future pandemics. Although SARS-CoV-2 usually accrues mutations slowly, it is likely that resistance will emerge to one or more of the antiviral drugs as the pandemic continues. Resistance to remdesivir owing to the selection of non-synonymous mutations in the nsp12-RdRp has recently been reported (Gandhi et al., 2022; Martinot et al., 2021; Stevens et al., 2022). The emergence of resistant strains can be delayed by giving the drugs in combination, as demonstrated by the long-term efficacy of multidrug treatments for HIV and HCV therapies.

Currently, remdesivir (GS-5734), molnupiravir (MK-4482), and paxlovid have been given EUA by the FDA for the treatment of COVID-19. Although similar to remdesivir, molnupiravir has been shown to function as an RNA mutagen (Sheahan et al., 2020), while remdesivir is a non-obligate RNA chain terminator (Warren et al., 2016). The function of molnupiravir as an RNA mutagen raises concerns regarding off-target mutagenic toxicity. In contrast, TEMPOL inactivates the RNA-dependent RNA polymerase of SARS-CoV-2 by causing the oxidative degradation of its two essential Fe-S metal cofactors (Maio et al., 2021) and it has no detectable cytotoxicity at doses up to 5 mM *in vitro* (Maio et al., 2021) and in prolonged treatments *in vivo* (Ghosh et al., 2008, 2018). Its reported 50% cytotoxic concentration is greater than 100 mM (Oliveira et al., 2019). A randomized, double-blind, placebo-controlled study in phase 2/3, sponsored by Adamis Pharmaceuticals Corporation and designed to examine the effects of TEMPOL in high-risk subjects with early COVID-19, is currently ongoing (NCT04729595, <https://clinicaltrials.gov/ct2/show/NCT04729595>). The trial offers TEMPOL, 400 mg orally twice a day for 14 days to patients with a recognized risk factor, within 5 days of baseline from a laboratory-confirmed infection with SARS-CoV-2. The primary outcome assessed will be the difference in the rate of sustained clinical resolution of COVID-19-related symptoms at day 14 compared to the placebo arm of the study. The secondary outcome will be the safety and efficacy of TEMPOL in reducing hospitalization and death. If the trial succeeds to enroll the approximately 248 patients the protocol was seeking to register, the study would provide the first line of evidence for the efficacy of TEMPOL against SARS-CoV-2 infection in humans, which is required to bring the drug into the clinic for the treatment of COVID-19. Preliminary results have not been reported yet.

Infectious disease pathophysiology results from a complex interplay between the pathogen and the host. Consequently, strategically planned combination therapies may be more effective than the use of single drugs for antiviral therapy in the initial stages of disease, and immunosuppressives to treat the acute distress respiratory syndrome that develops later in response to the initial infection. The combination of drugs with different mechanisms of action has been shown to be highly effective for the control of other pathogens, notably HIV and HCV infections (Maeda et al., 2019; Naggie and Muir, 2017).

In addition, immune response modifying drugs such as dexamethasone have been shown to be effective in the suppression of the later deleterious host immune responses associated with COVID-19 (Group et al., 2021). The combination of TEMPOL as a therapeutic with a direct antiviral activity with immune modulators may increase treatment efficacy, especially in more severe cases.

Our studies present evidence for pursuing TEMPOL—with its low cytotoxicity and known access to tissues relevant for SARS-CoV-2 infection (Cotrim et al., 2007; Wang et al., 2018)—and other related stable nitroxides as potential SARS-CoV-2 therapies during active viral infection. We propose that TEMPOL could be regarded as an antiviral that works through a different mechanism than other antivirals, and its likely low toxicity in humans could make it attractive for use as an oral post-exposure preventive treatment against SARS-CoV-2.

Limitations of the study

This study has two main limitations. First, the number of animals evaluated in this study for the analysis of the antiviral potency of TEMPOL against SARS-CoV-2 infection was small. Eight animals, comprising 4 males and 4 females, received TEMPOL, and eight (4 males and 4 females) were treated using the same route and timing as the TEMPOL group with vehicle only. A larger study would have enabled the

assessment of statistical significance of genome copy number and titer of infectious viruses in the upper respiratory tract (oropharyngeal swabs and nasal turbinates). Second, we could not perform a dose-response experiment to compare the effect of increasing concentrations of TEMPOL on titers of infectious virus in the upper respiratory tract and in the lungs and on the development of pathological signs in the lungs because of the limited availability of animals.

DATA AND MATERIALS AVAILABILITY

All data needed to evaluate the conclusions of the article are present in the main text and supplementary materials. All data reported in this article will be shared by the [lead contact](#) upon request. This study did not generate any new codes. Any additional information required to reanalyze the data reported in this work is available from the [lead contact](#) upon request.

STAR★METHODS

Detailed methods are provided in the online version of this paper and include the following:

- [KEY RESOURCES TABLE](#)
- [RESOURCE AVAILABILITY](#)
 - Lead contact
 - Materials availability
 - Data and code availability
- [EXPERIMENTAL MODEL AND SUBJECT DETAILS](#)
 - Virus
 - Cells
- [METHOD DETAILS](#)
 - Protocol for anti-SARS-CoV-2 testing in Calu-3 cells
 - Measurement of SARS-CoV-2, SARS-CoV and MERS-CoV viral inhibition in Vero 76 cells
 - Animals and study design
 - Syrian hamster study design
 - Experimental design
 - TCID₅₀ assay
 - Viral RNA extraction and quantification using qRT-PCR
 - Histopathology and immunohistochemistry
 - Experimental design
 - Severity grading scale
 - Immunohistochemistry
- [QUANTIFICATION AND STATISTICAL ANALYSIS](#)

SUPPLEMENTAL INFORMATION

Supplemental information can be found online at <https://doi.org/10.1016/j.isci.2022.105074>.

ACKNOWLEDGMENTS

The authors thank Dr. Ann Eakin, Senior Scientific Officer, NIH/NIAID/DMID, for guidance and support in using the NIAID antiviral resources, Drs. Bernard A. P. Lafont (NIAID), Daniel R. Crooks (NCI) and De-Liang Zhang (NICHD) for insightful discussions and technical assistance, Dr. Johnson Wang (VitroVivo Biotech, LLC) for the histological preparation and immunohistochemistry analysis of lung tissue specimens with anti-NP1 antibody, Dr. Swagata Kar, BIOQUAL and the histopathology group at EPL for their support with animal related work and for help with the display items, and the *Eunice Kennedy Shriver* National Institute of Child Health and Human Development for support. Funding: This work was supported by the Intramural Research Program of the National Institutes of Health (to T.A.R.) and by the Center for Cancer Research, National Cancer Institute (to W.M.L).

AUTHOR CONTRIBUTIONS

N.M., T.A.R., and W.M.L. conceived the project. N.M. contributed to the design, execution and data analysis, and writing of the article. S.C. and D.C.S. performed SARS-CoV-2 infection studies in Calu-3 cells. B.L.H. performed SARS-CoV-2, SARS-CoV, and MERS-CoV infection studies in Vero 76 cells. T.A.R. supervised the study and procured funds. N.M. performed and T.A.R. oversaw statistical analyses. N.M. and

T.A.R. had unrestricted access to all data. All authors analyzed the data, read, revised, and approved the final draft, and take full responsibility for the content and accuracy of the data.

DECLARATION OF INTERESTS

The authors declare that they have no competing interests.

Received: June 29, 2022

Revised: August 3, 2022

Accepted: August 31, 2022

Published: October 21, 2022

REFERENCES

- Chan, J.F.W., Zhang, A.J., Yuan, S., Poon, V.K.M., Chan, C.C.S., Lee, A.C.Y., Chan, W.M., Fan, Z., Tsoi, H.W., Wen, L., et al. (2020). Simulation of the clinical and pathological manifestations of coronavirus disease 2019 (COVID-19) in a golden Syrian hamster model: implications for disease pathogenesis and transmissibility. *Clin. Infect. Dis.* 71, 2428–2446. <https://doi.org/10.1093/cid/ciaa325>.
- WHO Solidarity Trial Consortium, Pan, H., Peto, R., Henao-Restrepo, A.M., Preziosi, M.P., Sathiyamoorthy, V., Abdool Karim, Q., Alejandria, M.M., Al-Bader, A.M., Kieny, M.P., et al. (2021). Repurposed antiviral drugs for covid-19 - interim WHO solidarity trial results. *N. Engl. J. Med.* 384, 497–511. <https://doi.org/10.1056/NEJMoa2023184>.
- Corman, V.M., Muth, D., Niemeyer, D., and Drosten, C. (2018). Hosts and sources of endemic human coronaviruses. *Adv. Virus Res.* 100, 163–188. <https://doi.org/10.1016/bs.aivir.2018.01.001>.
- Cotrim, A.P., Hyodo, F., Matsumoto, K.I., Sowers, A.L., Cook, J.A., Baum, B.J., Krishna, M.C., and Mitchell, J.B. (2007). Differential radiation protection of salivary glands versus tumor by Tempol with accompanying tissue assessment of Tempol by magnetic resonance imaging. *Clin. Cancer Res.* 13, 4928–4933. <https://doi.org/10.1158/1078-0432.CCR-07-0662>.
- Davis, R.M., Matsumoto, S., Bernardo, M., Sowers, A., Matsumoto, K.I., Krishna, M.C., and Mitchell, J.B. (2011). Magnetic resonance imaging of organic contrast agents in mice: capturing the whole-body redox landscape. *Free Radic. Biol. Med.* 50, 459–468. <https://doi.org/10.1016/j.freeradbiomed.2010.11.028>.
- Dittmar, M., Lee, J.S., Whig, K., Segrist, E., Li, M., Kamalia, B., Castellana, L., Ayyanathan, K., Cardenas-Diaz, F.L., Morrisey, E.E., et al. (2021). Drug repurposing screens reveal cell-type-specific entry pathways and FDA-approved drugs active against SARS-CoV-2. *Cell Rep.* 35, 108959. <https://doi.org/10.1016/j.celrep.2021.108959>.
- Edwards, A.M., Baric, R.S., Saphire, E.O., and Ulmer, J.B. (2022). Stopping pandemics before they start: lessons learned from SARS-CoV-2. *Science* 375, 1133–1139. <https://doi.org/10.1126/science.abn1900>.
- Gandhi, S., Klein, J., Robertson, A.J., Peña-Hernández, M.A., Lin, M.J., Roychoudhury, P., Lu, P., Fournier, J., Ferguson, D., Mohamed Bakhsh, S.A.K., et al. (2022). De novo emergence of a remdesivir resistance mutation during treatment of persistent SARS-CoV-2 infection in an immunocompromised patient: a case report. *Nat. Commun.* 13, 1547. <https://doi.org/10.1038/s41467-022-29104-y>.
- García-Beltrán, W.F., St Denis, K.J., Hoelzemer, A., Lam, E.C., Nitido, A.D., Sheehan, M.L., Berrios, C., Ofoman, O., Chang, C.C., Hauser, B.M., et al. (2022). mRNA-based COVID-19 vaccine boosters induce neutralizing immunity against SARS-CoV-2 Omicron variant. *Cell* 185, 457–466.e4. <https://doi.org/10.1016/j.cell.2021.12.033>.
- Ghosh, M.C., Tong, W.H., Zhang, D., Ollivierre-Wilson, H., Singh, A., Krishna, M.C., Mitchell, J.B., and Rouault, T.A. (2008). Tempol-mediated activation of latent iron regulatory protein activity prevents symptoms of neurodegenerative disease in IRP2 knockout mice. *Proc. Natl. Acad. Sci. USA* 105, 12028–12033. <https://doi.org/10.1073/pnas.0805361105>.
- Ghosh, M.C., Zhang, D.L., Ollivierre, H., Eckhaus, M.A., and Rouault, T.A. (2018). Translational repression of HIF2 α expression in mice with Chuvash polycythemia reverses polycythemia. *J. Clin. Invest.* 128, 1317–1325. <https://doi.org/10.1172/JCI97684>.
- Gordon, C.J., Tchesnokov, E.P., Schinazi, R.F., and Götte, M. (2021). Molnupiravir promotes SARS-CoV-2 mutagenesis via the RNA template. *J. Biol. Chem.* 297, 100770. <https://doi.org/10.1016/j.jbc.2021.100770>.
- Gordon, C.J., Tchesnokov, E.P., Woolner, E., Perry, J.K., Feng, J.Y., Porter, D.P., and Götte, M. (2020). Remdesivir is a direct-acting antiviral that inhibits RNA-dependent RNA polymerase from severe acute respiratory syndrome coronavirus 2 with high potency. *J. Biol. Chem.* 295, 6785–6797. <https://doi.org/10.1074/jbc.RA120.013679>.
- The RECOVERY Collaborative Group, Horby, P., Lim, W.S., Emberson, J.R., Mafham, M., Bell, J.L., Linsell, L., Staplin, N., Brightling, C., Ustianowski, A., et al. (2021). Dexamethasone in hospitalized patients with covid-19. *N. Engl. J. Med. Overseas Ed.* 384, 693–704. <https://doi.org/10.1056/NEJMoa2021436>.
- Huang, N., Pérez, P., Kato, T., Mikami, Y., Okuda, K., Gilmore, R.C., Conde, C.D., Gasmi, B., Stein, S., Beach, M., et al. (2021). SARS-CoV-2 infection of the oral cavity and saliva. *Nat. Med.* 27, 892–903. <https://doi.org/10.1038/s41591-021-01296-8>.
- Iketani, S., Liu, L., Guo, Y., Liu, L., Chan, J.F.W., Huang, Y., Wang, M., Luo, Y., Yu, J., Chu, H., et al. (2022). Antibody evasion properties of SARS-CoV-2 Omicron sublineages. *Nature* 604, 553–556. <https://doi.org/10.1038/s41586-022-04594-4>.
- Imai, M., Iwatsuki-Horimoto, K., Hatta, M., Loeber, S., Halfmann, P.J., Nakajima, N., Watanabe, T., Ujie, M., Takahashi, K., Ito, M., et al. (2020). Syrian hamsters as a small animal model for SARS-CoV-2 infection and countermeasure development. *Proc. Natl. Acad. Sci. USA* 117, 16587–16595. <https://doi.org/10.1073/pnas.2009799117>.
- Imlay, J.A. (2006). Iron-sulphur clusters and the problem with oxygen. *Mol. Microbiol.* 59, 1073–1082. <https://doi.org/10.1111/j.1365-2958.2006.05028.x>.
- Kumar, R., Lee, M.H., Mickael, C., Kassa, B., Pasha, Q., Tuder, R., and Graham, B. (2020). Pathophysiology and potential future therapeutic targets using preclinical models of COVID-19. *ERJ Open Res.* 6, 00405–02020. <https://doi.org/10.1183/23120541.00405-2020>.
- Lu, R., Zhao, X., Li, J., Niu, P., Yang, B., Wu, H., Wang, W., Song, H., Huang, B., Zhu, N., et al. (2020). Genomic characterisation and epidemiology of 2019 novel coronavirus: implications for virus origins and receptor binding. *Lancet* 395, 565–574. [https://doi.org/10.1016/S0140-6736\(20\)30251-8](https://doi.org/10.1016/S0140-6736(20)30251-8).
- Maeda, K., Das, D., Kobayakawa, T., Tamamura, H., and Takeuchi, H. (2019). Discovery and development of anti-HIV therapeutic agents: progress towards improved HIV medication. *Curr. Top. Med. Chem.* 19, 1621–1649. <https://doi.org/10.2174/1568026619666190712204603>.
- Majo, N., Lafont, B.A.P., Sil, D., Li, Y., Bollinger, J.M., Jr., Krebs, C., Pierson, T.C., Linehan, W.M., and Rouault, T.A. (2021). Fe-S cofactors in the SARS-CoV-2 RNA-dependent RNA polymerase are potential antiviral targets. *Science* 373, 236–241. <https://doi.org/10.1126/science.abi5224>.
- Martinot, M., Jary, A., Fafi-Kremer, S., Leducq, V., Delagrèverie, H., Garnier, M., Pacanowski, J., Mékinian, A., Pirenne, F., Tiberghien, P., et al. (2021). Emerging RNA-dependent RNA polymerase mutation in a remdesivir-treated B-cell immunodeficient patient with protracted coronavirus disease 2019. *Clin. Infect. Dis.* 73, e1762–e1765. <https://doi.org/10.1093/cid/ciaa1474>.

- Munster, V.J., Feldmann, F., Williamson, B.N., van Doremalen, N., Pérez-Pérez, L., Schulz, J., Meade-White, K., Okumura, A., Callison, J., Brumbaugh, B., et al. (2020). Respiratory disease in rhesus macaques inoculated with SARS-CoV-2. *Nature* 585, 268–272. <https://doi.org/10.1038/s41586-020-2324-7>.
- Naggie, S., and Muir, A.J. (2017). Oral combination therapies for hepatitis C virus infection: successes, challenges, and unmet needs. *Annu. Rev. Med.* 68, 345–358. <https://doi.org/10.1146/annurev-med-052915-015720>.
- Oliveira, L.B., Celes, F.S., Paiva, C.N., and de Oliveira, C.I. (2019). The paradoxical leishmanicidal effects of superoxide dismutase (SOD)-Mimetic tempol in leishmania braziliensis infection in vitro. *Front. Cell. Infect. Microbiol.* 9, 237. <https://doi.org/10.3389/fcimb.2019.00237>.
- Owen, D.R., Allerton, C.M.N., Anderson, A.S., Aschenbrenner, L., Avery, M., Berritt, S., Boras, B., Cardin, R.D., Carlo, A., Coffman, K.J., et al. (2021). An oral SARS-CoV-2 M(pro) inhibitor clinical candidate for the treatment of COVID-19. *Science* 374, 1586–1593. <https://doi.org/10.1126/science.abl4784>.
- Reed, L.J., and Muench, H. (1938). A simple method of estimating fifty percent endpoints. *Am. J. Epidemiol.* 27, 493–497. <https://doi.org/10.1093/oxfordjournals.aje.a118408>.
- Riva, L., Yuan, S., Yin, X., Martin-Sancho, L., Matsunaga, N., Pache, L., Burgstaller-Muehlbacher, S., De Jesus, P.D., Teriete, P., Hull, M.V., et al. (2020). Discovery of SARS-CoV-2 antiviral drugs through large-scale compound repurposing. *Nature* 586, 113–119. <https://doi.org/10.1038/s41586-020-2577-1>.
- Rosenke, K., Hansen, F., Schwarz, B., Feldmann, F., Haddock, E., Rosenke, R., Barbian, K., Meade-White, K., Okumura, A., Leventhal, S., et al. (2021). Orally delivered MK-4482 inhibits SARS-CoV-2 replication in the Syrian hamster model. *Nat. Commun.* 12, 2295. <https://doi.org/10.1038/s41467-021-22580-8>.
- Rosenke, K., Meade-White, K., Letko, M., Clancy, C., Hansen, F., Liu, Y., Okumura, A., Tang-Huau, T.L., Li, R., Saturday, G., et al. (2020). Defining the Syrian hamster as a highly susceptible preclinical model for SARS-CoV-2 infection. *Emerg. Microbes Infect.* 9, 2673–2684. <https://doi.org/10.1080/22221751.2020.1858177>.
- Rouault, T.A., and Maio, N. (2020). How oxidation of a unique iron-sulfur cluster in FBXL5 Regulates IRP2 levels and promotes regulation of iron metabolism proteins. *Mol. Cell* 78, 1–3. <https://doi.org/10.1016/j.molcel.2020.03.020>.
- Sauter, J.L., Baine, M.K., Butnor, K.J., Buonocore, D.J., Chang, J.C., Jungbluth, A.A., Szabolcs, M.J., Morjaria, S., Mount, S.L., Rekhtman, N., et al. (2020). Insights into pathogenesis of fatal COVID-19 pneumonia from histopathology with immunohistochemical and viral RNA studies. *Histopathology* 77, 915–925. <https://doi.org/10.1111/his.14201>.
- Schultz, D.C., Johnson, R.M., Ayyanathan, K., Miller, J., Whig, K., Kamalia, B., Dittmar, M., Weston, S., Hammond, H.L., Dillen, C., et al. (2022). Pyrimidine inhibitors synergize with nucleoside analogues to block SARS-CoV-2. *Nature* 604, 134–140. <https://doi.org/10.1038/s41586-022-04482-x>.
- Sheahan, T.P., Sims, A.C., Graham, R.L., Menachery, V.D., Gralinski, L.E., Case, J.B., Leist, S.R., Pyrc, K., Feng, J.Y., Trantcheva, I., et al. (2017). Broad-spectrum antiviral GS-5734 inhibits both epidemic and zoonotic coronaviruses. *Sci. Transl. Med.* 9, eaal3653. <https://doi.org/10.1126/scitranslmed.aal3653>.
- Sheahan, T.P., Sims, A.C., Zhou, S., Graham, R.L., Pruijssers, A.J., Agostini, M.L., Leist, S.R., Schäfer, A., Dinno, K.H., 3rd, Stevens, L.J., et al. (2020). An orally bioavailable broad-spectrum antiviral inhibits SARS-CoV-2 in human airway epithelial cell cultures and multiple coronaviruses in mice. *Sci. Transl. Med.* 12, eabb5883. <https://doi.org/10.1126/scitranslmed.abb5883>.
- Sheward, D.J., Kim, C., Ehling, R.A., Pankow, A., Castro Dopico, X., Dyrdak, R., Martin, D.P., Reddy, S.T., Dillner, J., Karlsson Hedestam, G.B., et al. (2022). Neutralisation sensitivity of the SARS-CoV-2 omicron (B.1.1.529) variant: a cross-sectional study. *Lancet Infect. Dis.* 00129–133. <https://doi.org/10.1016/S1473-3099>.
- Sia, S.F., Yan, L.M., Chin, A.W.H., Fung, K., Choy, K.T., Wong, A.Y.L., Kaewpreedee, P., Perera, R.A.P.M., Poon, L.L.M., Nicholls, J.M., et al. (2020). Pathogenesis and transmission of SARS-CoV-2 in golden hamsters. *Nature* 583, 834–838. <https://doi.org/10.1038/s41586-020-2342-5>.
- Stevens, L.J., Pruijssers, A.J., Lee, H.W., Gordon, C.J., Tchesnokov, E.P., Gribble, J., George, A.S., Hughes, T.M., Lu, X., Li, J., et al. (2022). Mutations in the SARS-CoV-2 RNA dependent RNA polymerase confer resistance to remdesivir by distinct mechanisms. *Sci. Transl. Med.* 14, eabo0718. <https://doi.org/10.1126/scitranslmed.abo0718>.
- Thompson, M.G., Natarajan, K., Irving, S.A., Rowley, E.A., Griggs, E.P., Gaglani, M., Klein, N.P., Grannis, S.J., DeSilva, M.B., Stenehjem, E., et al. (2022). Effectiveness of a third dose of mRNA vaccines against COVID-19-associated emergency department and urgent care encounters and hospitalizations among adults during periods of delta and omicron variant predominance - VISION Network, 10 states, august 2021-january 2022. *MMWR Morb. Mortal. Wkly. Rep.* 71, 139–145. <https://doi.org/10.15585/mmwr.mm7104e3>.
- Wang, Y., Hai, B., Ai, L., Cao, Y., Li, R., Li, H., and Li, Y. (2018). Tempol relieves lung injury in a rat model of chronic intermittent hypoxia via suppression of inflammation and oxidative stress. *Iran. J. Basic Med. Sci.* 21, 1238–1244. <https://doi.org/10.22038/ijbms.2018.31716.7714>.
- Warren, T.K., Jordan, R., Lo, M.K., Ray, A.S., Mackman, R.L., Soloveva, V., Siegel, D., Perron, M., Bannister, R., Hui, H.C., et al. (2016). Therapeutic efficacy of the small molecule GS-5734 against Ebola virus in rhesus monkeys. *Nature* 531, 381–385. <https://doi.org/10.1038/nature17180>.
- Wölfel, R., Corman, V.M., Guggemos, W., Seilmaier, M., Zange, S., Müller, M.A., Niemeyer, D., Jones, T.C., Vollmar, P., Rothe, C., et al. (2020). Virological assessment of hospitalized patients with COVID-2019. *Nature* 581, 465–469. <https://doi.org/10.1038/s41586-020-2196-x>.
- Woolsey, C., Borisevich, V., Prasad, A.N., Agans, K.N., Deer, D.J., Dobias, N.S., Heymann, J.C., Foster, S.L., Levine, C.B., Medina, L., et al. (2021). Establishment of an African green monkey model for COVID-19 and protection against re-infection. *Nat. Immunol.* 22, 86–98. <https://doi.org/10.1038/s41590-020-00835-8>.
- Yu, F., Yan, L., Wang, N., Yang, S., Wang, L., Tang, Y., Gao, G., Wang, S., Ma, C., Xie, R., et al. (2020). Quantitative detection and viral load analysis of SARS-CoV-2 in infected patients. *Clin. Infect. Dis.* 71, 793–798. <https://doi.org/10.1093/cid/ciaa345>.

STAR★METHODS

KEY RESOURCES TABLE

REAGENT or RESOURCE	SOURCE	IDENTIFIER
Antibodies		
Mouse anti-dsRNA J2	Absolute	Ab01299; RRID: AB_2923396
anti-Wuhan nucleocapsid (NP1) antibody	Genscript	SC1180-PU; Lot#: U393LGG200-4/DH0168
Bacterial and virus strains		
SARS-CoV-2 (USA-WA1/2020)	BEI	NR-52281
SARS-CoV (Urbani)	CDC	200300592
MERS-CoV (EMC/2012)	CDC	JX869059
Biological samples		
Hamster SARS-CoV2 infected lung tissue, fixed, embedded	Bioqual Inc.	N/A
Hamster SARS-CoV2 infected nasal turbinate, fixed, embedded	Bioqual Inc.	N/A
Oral swabs from Hamster	Bioqual Inc.	N/A
Chemicals, peptides, and recombinant proteins		
TEMPOL	SIGMA ALDRICH	8401300100
Critical commercial assays		
SuperScript™ III Reverse Transcriptase	ThermoFisher Scientific	12574026
QIAasymphony RNA Kit	QIAGEN	931636
MEGAscript T7 Transcription Kit	ThermoFisher Scientific	AM1334
MEGAclear Transcription Clean-UP Kit	ThermoFisher Scientific	AM1908
TapMan Fast Virus 1-Step Master Mix	ThermoFisher Scientific	4444432
ImmPRESS® HRP Goat Anti-Rabbit IgG Polymer Detection Kit	Vector Laboratories	MP-7451-50
Experimental models: Cell lines		
Calu-3	ATCC	HTB-55™
Vero 76	ATCC	CRL-1587™
Vero E6 _TMPRSS2_ACE2	BEI	NR-54970
Experimental models: Organisms/strains		
Golden Syrian hamster (<i>Mesocricetus auratus</i>)	Envigo	089
Oligonucleotides		
Primer: E_Sarbeco_R Reverse: ATATTGCAGC AGTACGCACACA	Wolfel et al., 2020	ThermoFisher Scientific:4448510
Probe:E_Sarbeco-6FAM/AC ACT AGC C/ZENA TCC TTA CTG CGC TTC G/IABkFQ	Wolfel et al., 2020	ThermoFisher Scientific:4448510
Primer:g_E_SARS-CoV-2-F ACA GGT ACG TTA ATA GTT AAT AGC GT	CDC Research Use Only 2019-Novel Coronavirus (2019-nCoV) Real-time RT-PCR Primers and Probes	ThermoFisher Scientific:4448510
Primer:g_E_SARS-CoV-2-R ATA TTG CAG CAG TAC GCA CAC A	CDC Research Use Only 2019-Novel Coronavirus (2019-nCoV) Real-time RT-PCR Primers and Probes	ThermoFisher Scientific:4448510
Primer:sgLeadSARS-CoV-2 Forward: CGATCT CTTGTAGATCTGTTCTC	Wolfel et al., 2020	ThermoFisher Scientific:4448510

(Continued on next page)

Continued

REAGENT or RESOURCE	SOURCE	IDENTIFIER
Primer:sgLeadSARS-CoV-2 Reverse: GGTGAA CCAAGACGCAGTAT	Wolfel et al., 2020	ThermoFisher Scientific:4448510
Probe:N- FAM-TAACCAGAATGGA GAACGCAGTG GG-BHQ1	Wolfel et al., 2020	ThermoFisher Scientific:4448510
Recombinant DNA		
Plasmid: pcDNA3.1+. SARS-CoV-2 N gene subgenomic RNA (sgRNA)	This study	N/A
Software and algorithms		
PRISM 8.4.3	GraphPad Software	N/A
PRISM 9.3.1	GraphPad Software	N/A
MetaXpress 5.3.3	Molecular Devices	N/A
QuantStudio Real-Time PCR Software v1.7.1	Life Technologies	N/A
ImageJ	National Institutes of Health	N/A

RESOURCE AVAILABILITY**Lead contact**

Further information and requests for resources and reagents should be directed to and will be fulfilled by the lead contact, Tracey A. Rouault (rouault@mail.nih.gov).

Materials availability

This study did not generate new unique reagents.

Data and code availability

- All data reported in this paper will be shared by the **lead contact**, Tracey A. Rouault (rouault@mail.nih.gov).
- This paper does not report original code.
- Any additional information required to reanalyze the data reported in this paper is available from the **lead contact**, Tracey A. Rouault (rouault@mail.nih.gov), upon request.

EXPERIMENTAL MODEL AND SUBJECT DETAILS**Virus**

SARS-CoV-2 (USA-WA1/2020; Biodefense and Emerging Infections Research Resources Repository (BEI Resources), #NR-52281; 1.2×10^6 TCID₅₀/mL) challenge stock was grown in Calu-3 cells [American Type Culture Collection (ATCC) #HTB-55]. Full genome sequencing revealed 100% identity with the parent virus sequence (GenBank MN985325.1; courtesy David O'Connor, Shelby O'Connor, University of Wisconsin).

Cells

Vero 76 cells for antiviral testing against SARS-CoV-2 (strain: USA-WA1/2020), SARS-CoV (strain: Urbani) and MERS-CoV (strain: EMC) were purchased from ATCC (ATCC # CRL-1587™) and propagated in Dulbecco's modified Eagle's medium (DMEM) with 4.5 g/L glucose, supplemented with 10% fetal bovine serum (FBS) and 2 mM glutamine at 37°C and 5% CO₂ in a humidified incubator.

Calu-3 cells [American Type Culture Collection (ATCC) #HTB-55] were grown in Minimal Eagle's Medium supplemented with 1% non-essential amino acids, 1% penicillin/streptomycin, and 10% FBS at 37°C and 5% CO₂ in a humidified incubator.

METHOD DETAILS

Protocol for anti-SARS-CoV-2 testing in Calu-3 cells

Calu-3 cells (ATCC, HTB-55) grown in Minimal Eagle's Medium supplemented with 1% non-essential amino acids, 1% penicillin/streptomycin, and 10% FBS are plated in 384 well plates. The next day, 50 nL of TEMPOL suspended in DMSO was added as an 8-pt dose response with three-fold dilutions between test concentrations in triplicate, starting at 20 μ M final concentration. The negative control (DMSO, n = 32) and positive control (10 μ M Remdesivir, n = 32) are included on each assay plate. Calu3 cells are pre-treated with controls and test drugs (in triplicate) for 2 h prior to infection. In BSL3 containment, SARS-CoV-2 (isolate USA WA1/2020) diluted in serum free growth medium was added to assay plates to achieve an MOI = 0.5. Cells were incubated continuously with drugs and SARS-CoV2 for 48 h. Cells were fixed and then immunostained with anti-dsRNA (mAb, J2) and nuclei were counterstained with Hoechst 33,342 for automated microscopy. Automated image analysis quantified the number of cells per well (toxicity) and the percentage of infected cells (dsRNA + cells/cell number) per well. SARS-CoV-2 infection at each drug concentration was normalized to aggregated DMSO plate control wells and expressed as percentage-of-control (POC = % Infection_{sample}/Avg % Infection_{DMSO cont}). A non-linear regression curve fit analysis (GraphPad Prism 8) of POC Infection and cell viability versus the log₁₀ transformed concentration values was used to calculate IC₅₀ values for Infection and CC₅₀ values for cell viability. Selectivity index (SI) was calculated as a ratio of drug's CC₅₀ and IC₅₀ values (SI = CC₅₀/IC₅₀) (Dittmar et al., 2021; Schultz et al., 2022).

Measurement of SARS-CoV-2, SARS-CoV and MERS-CoV viral inhibition in Vero 76 cells

These assays were performed at the Institute for Antiviral Research of Utah State University under contracts sponsored by NIAID. SARS coronavirus (strain: Urbani) was tested in Vero 76 cells (ATCC CRL-1587™), with M128533, an inhibitor of the main protease, being used as a positive control drug at 0.1-100 μ g/mL. MERS coronavirus (strain: EMC) was tested in Vero 76 cells, with M128533 being used as a control drug at 0.1-100 μ g/mL. SARS-CoV-2 (strain: USA-WA1/2020) was tested in Vero 76 cells, with EIDD-1931, a ribonucleoside analog, being used as a positive control drug at 0.1-100 μ g/mL. TEMPOL was dissolved in DMSO and tested in the concentration range of 25-1000 μ M for SARS-CoV-2 and MERS-CoV and 0.1-100 μ M for SARS-CoV, with DMSO being used as a vehicle control. Visual inspection and neutral red assay were used to measure cytopathic effect and toxicity. EC₅₀ and CC₅₀ values were extracted from primary data. EC₅₀ and CC₅₀ results from visual inspection and neutral red assay were consistent. Representative results of both assays were reported in the paper. EC₅₀ of control drugs on MERS-CoV, SARS-CoV and SARS-CoV-2 were 0.28 μ M, 0.67 μ M and 0.3 μ M, respectively, based on neutral red staining (see Table S1).

Animals and study design

Six-to-eight-week-old, inbred female and male golden Syrian hamsters (*Mesocricetus auratus*) (Envigo) were randomly allocated to the vehicle control or TEMPOL-treated group (n = 8 per group) and infected with SARS-CoV-2 (USA-WA1/2020) in a volume of 100 μ L (50 μ L/nostril) by the intranasal route. Hamsters were healthy and drug-naïve with no history of previous procedures. Following challenge, body weights were assessed daily. Body weight loss that exceeded 20% of the weight on the day of challenge was established as a humane endpoint criterion for euthanasia. A subset of 4 animals per group were necropsied on day 4 and a subset of 4 per group at day 10 for viral loads and histopathology. All animal studies were conducted in compliance with all relevant local, state, and federal regulations and were approved by the Bioqual Institutional Animal Care and Use Committee (IACUC).

Syrian hamster study design

A total of sixteen Golden Syrian hamsters were on study. Animals were intranasally challenged with SARS-CoV-2 on Study Day (SD) 0. Animals were separated into two groups (n = 8 per group; 4 males and 4 females), a vehicle control and a TEMPOL treated group that received subcutaneous injections in the interscapular area. Two animals per group and sex were sacrificed at two timepoints, SD 4 and SD 10. See Experimental Design, Text Table 1.

Experimental design

Group	N	Treatment (SQ)	Dose	Tx Days	Challenge (IN)	Weights and Clinical Observations ^a	Blood Collection (SST) ^b	Oral Swabs	Tissue Collection ^c
1	8 (4F/4M)	Vehicle Control	1.5 mL	2 HR pre-Challenge BID on SD 1-3	SD 0: SARS-CoV-2	Daily weights and BID observations during challenge period	Pre-Treatment	SD 2, 4, 7, 10 (TCID ₅₀)	2/grp/sex on SD 4, 10: Collect lungs and nasal turbinates
2	8 (4F/4M)	TEMPOL	50 or 25 mg/kg in 1.5 mL	SID on SD 4-9		COVID scoring during AM observations	Pre-Challenge on SD 0, Max Bleed at Termination		

IN; intranasal.

^aObserve animals once on each day blood is collected or animals are anesthetized. Observe twice daily during challenge period.

^bBlood processing and assay instructions.

^cLeft lungs were preserved in 10% NBF for histopathology. Right lungs and nasal turbinates 1 section (0.05-0.1g) were snap frozen for PCR and 1 section (0.1-0.2g) snap frozen for TCID₅₀.

TCID₅₀ assay

For infectious titer determination from tissue samples, TCID₅₀ assay was performed. To set up the assay, frozen lung tissue was placed in a 15 mL conical tube on wet ice containing 0.5 mL media and homogenized 10-30 s (Probe, Omni International: 32750H). For the nares, 1 mL media was used for homogenizing the tissues for 10-30 s. The tissue homogenate was spun to remove debris at 2000 x g at 4°C for 10 min. The supernatant was passed through a strainer. 20 µL of the supernatant was tested in the assay in quadruplicate in a 96-well plate format.

For the TCID₅₀, Vero TMPRSS2 cells were plated at 25,000 cells per well in DMEM +10% FBS + Gentamicin. The plate was incubated at 37°C, 5% CO₂. Cells were 80-100% confluent the following day. The media was aspirated and replaced with 180 µL of DMEM +2% FBS + gentamicin. 20 µL of sample was added to the top row in quadruplicate. The top row was mixed 5 times with a pipette and titered down to generate 10-fold dilutions. The pipette tips were disposed of between each row and the mixing was repeated until the last row on the plate was completed. The plates for the samples were incubated again at 37°C, 5% CO₂ for 4 days. After 4 days, the plates were visually inspected for cytopathic effect (CPE). The presence of CPE was recorded as a plus (+) and absence of CPE as minus (-). The TCID₅₀ was then calculated using the Read-Muench formula (Reed and Muench, 1938).

For optimal assay performance, the TCID₅₀ of the positive control should test within 2-fold of the expected value.

Viral RNA extraction and quantification using qRT-PCR

Genomic RNA amplification

The assay for SARS-CoV-2 qPCR was designed to detect total RNA using the WHO primer/probe set E_Sarbeco (Charité/Berlin). A QIAasymphony SP (QIAGEN, Hilden, Germany) automated sample preparation platform along with a virus/pathogen DSP midi kit and the *complex800* protocol were used to extract viral RNA from 800 µL of each sample. A reverse primer specific to the envelope (E) gene of SARS-CoV-2 (5'-ATA TTG CAG CAG TAC GCA CAC A-3') was annealed to the extracted RNA and then reverse transcribed into cDNA using SuperScript III Reverse Transcriptase (Thermo Fisher Scientific, Waltham, MA) along with RNase Out (Thermo Fisher Scientific, Waltham, MA). The resulting cDNA was treated with RNase H (Thermo Fisher Scientific, Waltham, MA) and then added to a custom 4x TaqMan Gene Expression Master Mix (Thermo Fisher Scientific, Waltham, MA) containing primers and a fluorescently labeled hydrolysis probe specific for the envelope gene of SARS-CoV-2 (forward primer 5'-ACA GGT ACG TTA ATA GTT AAT AGC GT-3', reverse primer 5'-ATA TTG CAG CAG TAC GCA CAC A-3', probe 5'-6FAM/AC ACT AGC C/ZENA TCC TTA CTG CGC TTC G/IABkFQ-3'). The qPCR was carried out on a QuantStudio 3 Real-Time PCR System (Thermo Fisher Scientific, Waltham, MA). SARS-CoV-2 RNA copies per reaction were interpolated using quantification cycle data and a serial dilution of a highly characterized custom DNA plasmid containing the SARS-CoV-2 envelope gene sequence. Mean RNA copies per milliliter were then calculated by applying the assay dilution factor (DF = 11.7). The limit of detection (LOD) for this assay was approximately 62 RNA copies per mL of sample.

Subgenomic RNA amplification

SARS-CoV-2 nucleocapsid (N) gene sub-genomic mRNA (sgRNA) was measured by a one-step RT-qPCR adapted from previously described methods (Wolfel et al., 2020; Yu et al., 2020). To generate standard curves, the SARS-CoV-2 N gene sgRNA sequence, including the 5'UTR leader sequence, transcriptional regulatory sequence (TRS), and the first 227 bp of the N gene, was cloned into a pcDNA3.1 plasmid. The pcDNA3.1 plasmids were linearized, transcribed using MEGAscript T7 Transcription Kit (ThermoFisher, Catalog # AM1334), and purified with MEGAclear Transcription Clean-Up Kit (ThermoFisher, Catalog # AM1908). The purified RNA products were quantified on Nanodrop, serially diluted, and aliquoted as N sgRNA standards.

RNA extracted from animal samples or standards were then measured in Taqman custom gene expression assays (ThermoFisher Scientific). For these assays, TaqMan Fast Virus 1-Step Master Mix (ThermoFisher, catalog # 4444432) and custom primers/probes targeting the N gene sgRNA (forward primer: 5'-CGATCTCTGTAGATCTGTTCTC -3'; reverse primer: 5'-GGTGAA CCAAGACGCAGTAT -3'; probe: 5'-FAM-TAACCAGAATGGAGAACGCAGTG GG-BHQ1 3') were used. RT-qPCR reactions were carried out

on a QuantStudio 3 Real-Time PCR System (Applied Biosystems) or a StepOnePlus Real-Time PCR System (Applied Biosystems) using the program below: reverse transcription at 50°C for 5 min, initial denaturation at 95°C for 20 s, followed by 40 cycles of denaturation-annealing-extension at 95°C for 15 s and 60°C for 30 s, respectively. Standard curves were used to calculate N sgRNA in copies per mL; the limit of detections (LOD) for N sgRNA assays were 12.5 copies per reaction or 150 copies per mL.

Histopathology and immunohistochemistry

Histopathology evaluation of hamsters and lung sections were performed by Experimental Pathology Laboratories, Inc. (Sterling, VA). Two animals per group and sex were sacrificed at two timepoints, Study Day (SD) 4 and SD 10. See [Experimental Design](#), Text Table 2.

Experimental design

Group	N	Treatment (SQ)	Dose	TX Days	SD 0 - Challenge (IN)	Tissue Collection
1	8 (4M/4F)	Vehicle control	1.5 mL	2 HR pre-Challenge,	SD 0: SARS-CoV-2	2/grp/sex on SD 4, 10: left lung in
2	8 (4M/4F)	TEMPOL	50 mg/ kg in 1.5 mL	BID on SD 1-3, SID on SD 4-9		10% NBF for histology

*NBF, neutral buffered formalin; M, male; F, female; HR, hour; SQ, subcutaneous; TX, treatment.

At necropsy, lung was collected and placed in 10% neutral buffered formalin for histopathologic analysis. Fixed tissues were processed to hematoxylin and eosin-stained slides and examined by a board-certified pathologist at Experimental Pathology Laboratories, Inc. (EPL) in Sterling, Virginia.

Severity grading scale

The severity of the non-neoplastic tissue lesions was graded as follows:

- Grade 1 (1+): Minimal. This corresponds to a histopathologic change ranging from inconspicuous to barely noticeable but so minor, small, or infrequent as to warrant no more than the least assignable grade. For multifocal or diffusely-distributed lesions, this grade was used for processes where less than approximately 10% of the tissue in an average high-power field was involved. For focal or diffuse hyperplastic/hypoplastic/atrophic lesions, this grade was used when the affected structure or tissue had undergone a less than approximately 10% increase or decrease in volume.
- Grade 2 (2+): Mild. This corresponds to a histopathologic change that is a noticeable but not a prominent feature of the tissue. For multifocal or diffusely-distributed lesions, this grade was used for processes where between approximately 10 and 25% of the tissue in an average high-power field was involved. For focal or diffuse hyperplastic/hypoplastic/atrophic lesions, this grade was used when the affected structure or tissue had undergone between an approximately 10%–25% increase or decrease in volume.
- Grade 3 (3+): Moderate. This corresponds to a histopathologic change that is a prominent but not a dominant feature of the tissue. For multifocal or diffusely-distributed lesions, this grade was used for processes where between approximately 25 and 50% of the tissue in an average high-power field was involved. For focal or diffuse hyperplastic/hypoplastic/atrophic lesions, this grade was used when the affected structure or tissue had undergone between an approximately 25%–50% increase or decrease in volume.
- Grade 4 (4+): Marked. This corresponds to a histopathologic change that is a dominant but not an overwhelming feature of the tissue. For multifocal or diffusely-distributed lesions, this grade was used for processes where between approximately 50 and 95% of the tissue in an average high-power field was involved. For focal or diffuse hyperplastic/hypoplastic/atrophic lesions, this grade was used when the affected structure or tissue had undergone between an approximately 50%–95% increase or decrease in volume.
- Grade 5 (5+): Severe. This corresponds to a histopathologic change that is an overwhelming feature of the tissue. For multifocal or diffusely-distributed lesions, this grade was used for processes where greater than approximately 95% of the tissue in an average high-power field was involved. For focal or diffuse hyperplastic/hypoplastic/atrophic lesions, this grade was used when the affected structure or tissue had undergone a greater than approximately 95% increase of decrease in volume.

Immunohistochemistry

Immunohistochemistry with anti-Wuhan nucleocapsid (NP1) antibody (GenScript Cat#: SC1180-PU; Lot#: U393LGG200-4/DH0168) was performed by VitroVivo Biotech, LLC (Rockville, MD). Formalin-fixed paraffin embedded section slides at 4 μm were immersed in citrate buffer (pH 6.0) microwaved for 3 min, then steamed at 95°C for 15 min for antigen retrieval. Blocking was performed with PBS with normal goat serum. Incubation with the primary antibody was done overnight at 4°C. Serial dilutions were tested (1:125; 1:250; 1:500; 1:1000; 1:2000; 1:4000 and 1:8000). Optimal dilution of the primary antibody was 1:4000. Endogenous peroxidase blocking was performed with 1% H_2O_2 in PBS for 15 min. Detection was done with ImmPRESS-HRP goat anti-rabbit IgG polymer for 60 min at RT. Tissues were then processed for immunohistochemistry with 25 μL stock diaminobenzidine (DAB) in 1 mL DAB buffer plus H_2O_2 for 2 min. Counterstaining was performed with Mayer's hematoxylin solution for 60 s.

QUANTIFICATION AND STATISTICAL ANALYSIS

Statistical analyses were performed in Prism 9 (GraphPad). Parametric, unpaired, two tailed t-tests with Welch's correction were used to assess significance between two groups (vehicle vs TEMPOL-treated).